Laser Initiation Processes in Thermite Energetic Materials Using Laser Desorption Ionization Time-of-Flight Mass Spectrometry

ARTICLE *in* THE JOURNAL OF PHYSICAL CHEMISTRY C · OCTOBER 2007

Impact Factor: 4.77 · DOI: 10.1021/jp076092x

3 AUTHORS, INCLUDING:

A. E. Stiegman
Florida State University
109 PUBLICATIONS **2,226** CITATIONS

Laser Initiation Processes in Thermite Energetic Materials Using Laser Desorption Ionization Time-of-Flight Mass Spectrometry

Melissa L. Mileham,[†] Michael P. Kramer,[‡] and A. E. Stiegman*[,†]

Department of Chemistry and Biochemistry, Florida State University, Tallahassee, Florida 32306, and AFRL/MNME, Eglin AFB, Florida 32542

Received: July 31, 2007; In Final Form: August 29, 2007

The reactive processes that occur during the laser initiation of aluminum/iron(III) oxide metastable intermolecular composites (MIC) have been studied by laser-induced desorption ionization time-of-flight mass spectrometry. The ions observed in the plume from the aluminum show fragments from the ablation of the oxide coating and from the metal core. Ablation of the iron oxide component consists primarily of pure iron species such as $[Fe]^+$ and $[Fe_2]^+$ and small oxides such as $[FeO]^+$ and $[Fe_2O]^+$ ions. In smaller quantities, metal oxide clusters that are either oxygen deficient, $[Fe(FeO)_x]^+$, or oxygen equivalent, $[(FeO)_x]^+$, are observed. When the thermite composite is initiated, mixed metal species are observed in the plume, which correspond to the aluminum substitution analogues of the iron oxide clusters, specifically, $[FeAl_2O_3]^+$, $[AlFe_2O_3]^+$, and $[AlFe_2O_2]^+$. Notably, the amounts of these mixed metal products that form are inversely proportional to the size of the aluminum particles. This suggests that the decrease in ignition time observed in MIC materials is due to the more facile liberation of reactive metallic aluminum when the particle size is small.

Introduction

Binary solid-state inorganic fuel/oxidant redox processes typified by the classic aluminum/iron oxide thermite reaction (eq 1) are of interest for the production of energetic materials because of their very high energy densities.[1]

$$2Al + Fe_2O_3 \rightarrow Al_2O_3 + 2Fe \quad (1)$$

Traditionally, these materials have not been broadly useful because mass-transport processes in the solid state mediate the rate of energy release so the power obtained is lower than that needed for certain applications. Recently, it has been determined that many of the desired energetic properties can be greatly enhanced when at least one of the component phases has dimensions in the nanometer size range. The rapid energy release processes in these materials, referred to as metastable interstitial composites (MIC), have been attributed to more intimate fuel/oxidizer contact occurring at the nanoscale, which enhances mass transport and provides more power.[2,3]

Studies of standard binary fuel−oxidant energetic materials typically involve thermochemical measurements such as temperature profiles, burn rates, or non-isothermal calorimetry (i.e., DSC, DTA, or TGA).[4−6] More recently, in studies of MIC materials, the use of laser-induced photothermal initiation has been exploited to allow instantaneous coupling of high-speed cameras for quantitative determination of properties such as the ignition time and the burn rate. These studies have been essential in quantifying the effect of particle size on combustion properties.[7−9]

Thermal initiation of thermite materials typically involves heating above the melting point of one of the components (usually the metal).[1] This starts the reaction processes that liberate heat, causing the reaction to accelerate. Ignition occurs when the reaction becomes self-sustaining and propagates. For laser initiation, the incident energy put into the sample by the laser causes high localized heating, which leads to ignition of the bulk. The time to ignition is defined as the time at which the energy released by the reaction becomes greater than or equal to the energy put into the composite by the laser. Both the laser excitation event and the subsequent ignition and propagation of the mixture are extremely high-temperature events which generate both liquid- and gas-phase (plasma) species. Chemical reactions between species occurring within and between these phases and with the solid material all contribute to the net combustion process.[9] This complexity coupled with the high temperatures makes these reactions difficult to study on a microscopic level. This has been addressed recently by the use of time-resolved spectroscopy. In particular, Dlott et al. have initiated the reaction between aluminum and nitrocellulose by flash-heating with a 100 ps laser pulse in the near infrared.[10,11] Short-pulse photothermal initiation allows the use of time-resolved spectroscopic techniques to monitor reaction dynamics, elucidate some of the intermediate species produced during the reaction, and to observe specific structural changes in the reactive components. Additionally, time-resolved studies of combusting Al/MoO_3 MIC composites have identified neutral species such as AlO formed in the process.[12]

We report the application of photothermal laser initiation coupled with time-of-flight mass spectrometry (LDI/TOF-MS) to directly observe ionic species that occur in the plasma phase of conventional Al/Fe_2O_3 thermite and the corresponding MIC materials during the laser incidence event. To the best of our knowledge, this is the first use of this technique to characterize reactive species in the initiation phase of binary inorganic reactions.

* To whom correspondence should be addressed. E-mail: stiegman@chem.fsu.edu.
[†] Florida State University.
[‡] Eglin AFB.

10.1021/jp076092x CCC: $37.00
Published on Web 10/19/2007

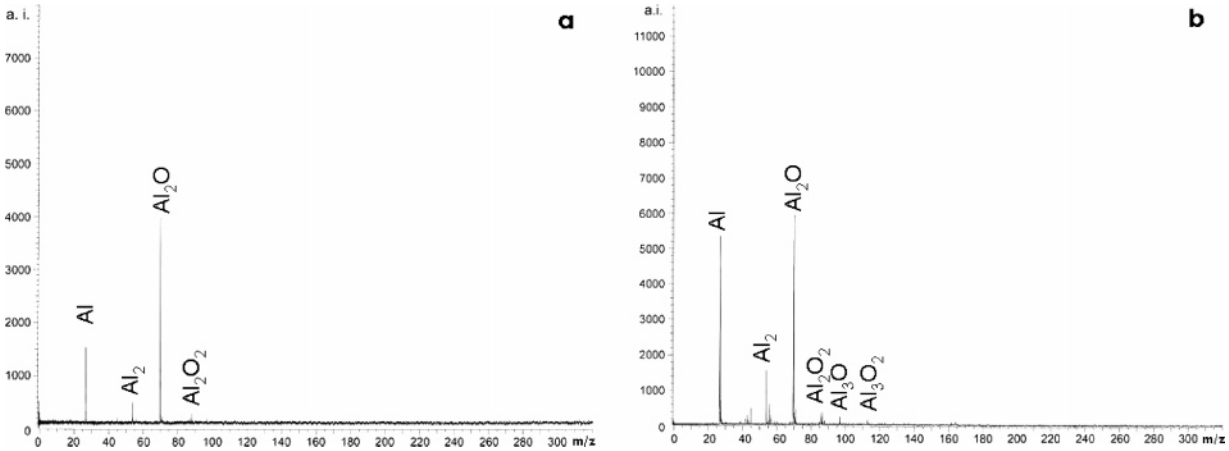

Figure 1. LDI−TOF mass spectra of 50 nm aluminum at a laser energy density of (a) 1.74 and (b) 1.90 J/cm^2.

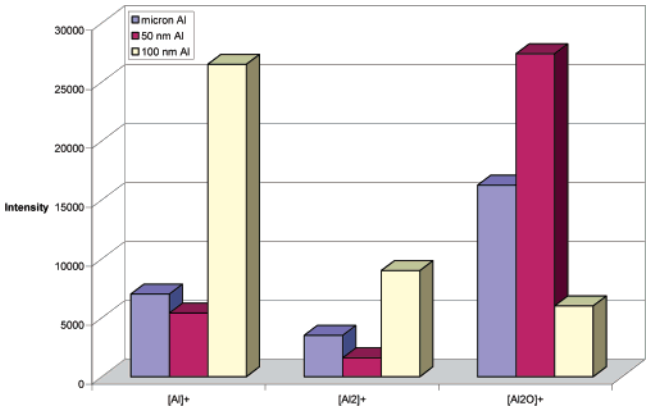

Figure 2. Aluminum ions formed at a laser energy density of 1.90 J/cm^2 for each aluminum particle size.

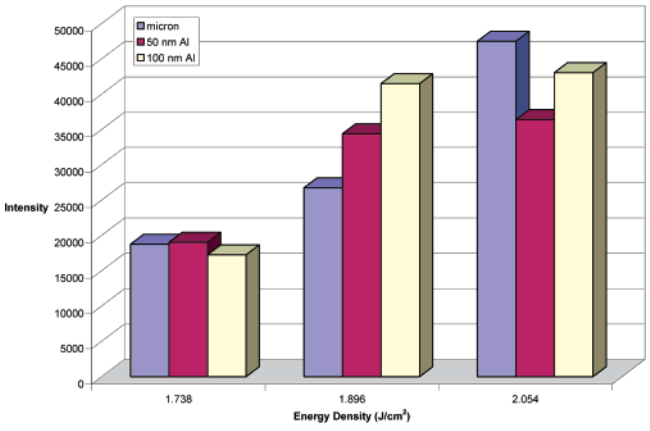

Figure 3. Major aluminum ions formed ($[Al^+] + [Al_2]^+ + [Al_2O]^+$) for each particle size at increasing energy densities.

Experimental Section

Materials: The 50 and 100 nm aluminum samples were obtained from Argonide, while the micron aluminum was purchased from Alfa Aesar. All aluminum samples were used as received. The iron(III) oxide powder, <0.25 μm, was purchased from Aldrich and was used as received.

The size and morphology of the aluminum samples were characterized by field emission scanning electron microscopy. The nanoscale materials are somewhat polydispersed, with the average particle size being around 50 and 100 nm for the two sizes, although both showed some particles above 200 and below 50 nm. Both samples showed some agglomeration of the particles, which was more pronounced in the 50 nm material. The aluminum, which we designate as "micron" scale, was a very polydispersed material composed largely of particles between 0.5 and 2.5 μm in size with only a few large particles around 5 μm observable. The average size of the micron sample, averaged from the particles observable in the SEM, was 1.75 μm. The active aluminum content and the estimated oxide thickness for the three samples were determined from weight gain measurements using thermogravimetric analysis. The active Al content for the 50 and 100 nm and the 2.5 μm materials was 71.5, 75.5, and 98.0%, respectively, while the oxide thickness was determined to be 2.6, 4.5, and 6.0 nm, respectively.

Preparation of Samples: The thermite samples were prepared by mixing Fe_2O_3 with each of the aluminum particles at a 2:1 molar aluminum to iron ratio. The samples were thoroughly mixed by grinding the components using a mortar and pestle to ensure a homogeneous distribution. Analysis of the samples after grinding using powder X-ray diffraction indicated that no new phases were formed as a result of sample preparation. The samples were then packed into a sample holder for laser desorption ionization time-of-flight mass spectrometry (LDI/TOF-MS) along with the control samples of Fe_2O_3 and the 50 and 100 nm and the micron aluminum.

Instrumentation: The LDI/TOF mass spectra were collected using a commercial 1999 Bruker Biflex III matrix-assisted laser desorption and ionization time-of-flight mass spectrometer (MALDI−TOF) (Bruker Daltronics, Inc.) fitted with a solid sample holder for the introduction of inorganic material. The instrument was equipped with a pulsed nitrogen laser at 337 nm with a peak width of 4 ns. All spectra were collected in linear mode with positive ion detection averaging 200 shots from the laser.

The reflectivity of the independent Al and Fe_2O_3 components and the compounded thermite were measured as total reflectance against a calibrated Spectralon diffuse scattering reference in a Perkin-Elmer Lambda 900 spectrophotometer equipped with a 160 mm integrating sphere.

In order to thermally initiate thermite, temperatures at or above the melting point of aluminum must be obtained. For laser pulses in the nanosecond regime, there is enough time for thermal transport into the material. The temperature attained in each component of the thermite can be estimated from the absorbed energy per unit volume, E_v, using eq 2, where J is the

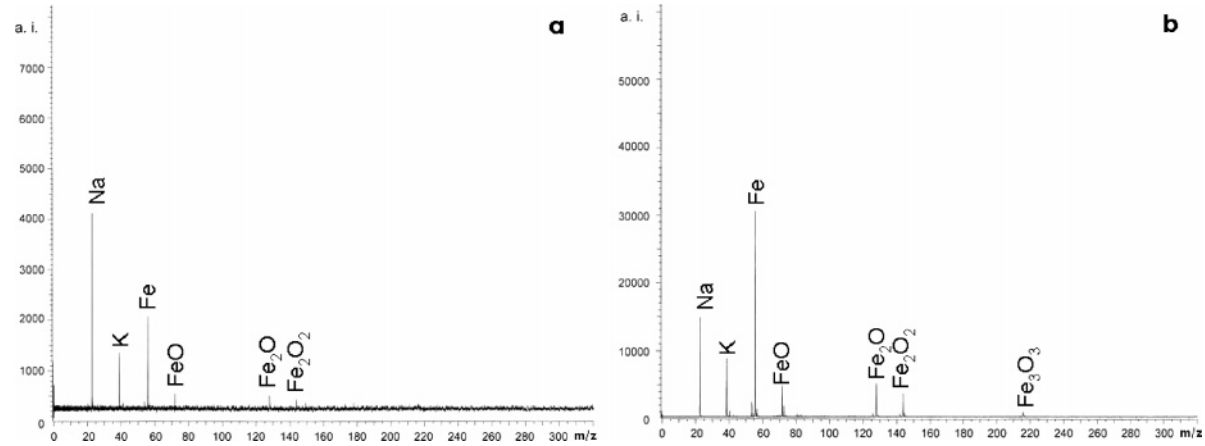

Figure 4. LDI−TOF mass spectra of iron(III) oxide at a laser energy density of (a) 1.58 and (b) 1.74 J/cm^2.

fluence at the center of the beam, R is the reflection coefficient, Λ_D is the thermal diffusion length, which is the depth of the sample that is heated with a single pulse from the laser, $C(T)$ is the heat capacity, and ρ is the density. The thermal diffusion length is calculated from the thermal diffusivity (D) and the pulse length of the laser (eq 3).[10,11,13]

$$E_v = J(1 - R)/\Lambda_D = \rho \int_{T_i}^{T_f} C(T)\mathrm{d}T \quad (2)$$

$$\Lambda_D = \frac{1}{2}(2\pi Dt)^{1/2} \quad (3)$$

It was found that all of the aluminum was melted when the laser reached an energy density of 0.158 J/cm^2. The volume of aluminum that was heated per pulse was approximately 7.42 × 10^{-9} cm^3. Although the volume of the sample that was hit by the laser did not change, the active aluminum content would vary based on the size of the aluminum particle. The Fe_2O_3 phase of the composite also absorbed at 337 nm and was found to reach its melting point of 1565 °C at an energy density of 0.474 J/cm^2. Temperatures required to generate a plume from which species could be detected in TOF-MS were found to be above these threshold values of melting.

Results and Discussion

Aluminum samples in the three particles sizes, 3−5 μm and 50 and 100 nm, were placed as tightly pressed powders in the laser desorption ionization instrument. Time-of-flight mass spectra observed for the 50 nm Al as a function of incident laser power are shown in Figure 1. No gas-phase ionic products were observed below a threshold energy density of 0.948 J/cm^2. Above this threshold, the major products included $[Al]^+$, $[Al_2O]^+$, and $[Al_2]^+$ at m/z of 26.9, 69.9, and 53.9, respectively. At power densities between 1.74 and 1.90 J/cm^2, small amounts of more complex Al_xO_y products were also observed, including $[Al_2O_2]^+$, $[Al_3O]^+$, and $[Al_3O_2]^+$ at m/z 85.9, 96.9, and 113, respectively (Figure 1b). Since the system was evacuated, the oxide species must have originated either directly or indirectly from the native oxide layer on the aluminum powder. Laser desorption of Al_2O_3 produced a large number of neutral species, with the dominant ones being AlO, Al_2O, and Al_2O_2.[14,15] In fact, AlO has been observed in the emission spectrum of combusting Al/MoO_3 thermite materials.[12] Since the observed aluminum oxide ion clusters are oxygen deficient, they are likely formed from ion−molecule reactions in the plasma between Al^+ and neutrals such as those given in eqs 4−6. Clearly, other pathways may also be operating. The species AlO^+ and $Al_2O_2^+$ are only observed at a higher laser power and may represent direct ion yields from ablation of the Al_2O_3 layer.

$$Al^+ + AlO \rightarrow Al_2O^+ \quad (4)$$

$$Al^+ + Al_2O \rightarrow Al_3O^+ \quad (5)$$

$$Al^+ + Al_2O_2 \rightarrow Al_3O_2^+ \quad (6)$$

Studies by Granier and Pantoya on the fuel particle size dependence of laser ignition of Al/MoO_3 MIC materials showed a general trend of faster ignition times as the Al particle size dropped to nanometer dimensions.[8] This effect was attributed to melting point depression that accompanies the size reduction in the aluminum. Also important in the laser ignition process is the presence of a native oxide layer on the aluminum. The oxide layer is thickest on micron-size Al and decreases to ∼2−4.5 nm as the Al particle size reaches the nanometer dimension. Notwithstanding the thinner oxide layer, the percent of active Al metal available will also decrease (i.e., Al_2O_3 represents a progressively higher percent of the mass of the particle). A direct effect of this is a reduction of the burn rate at very small particle sizes. The process of laser initiation will involve melting of the aluminum, the density change of which is sufficient to critically stress and break the oxide layer.[16] As indicated above, the ions that are observed in the plasma can be associated with both the oxide and the aluminum phase of the nanoparticles. Since the oxide has an extremely high melting point and a weak optical absorption, most of the heating during the pulse will be of the metal itself. Above the energy density threshold, the three dominant species are $[Al]^+$, $[Al_2]^+$, and $[Al_2O]^+$, which reflect contributions from the volatilization and ionization of the Al metal and the breakdown of the aluminum oxide shell. The amounts of these species observed for all three Al particle sizes at an energy density of 1.90 J/cm^2 are shown in Figure 2. The 100 nm particles show a large yield of $[Al]^+$ and a small yield of $[Al_2O]^+$, while the converse is true for the 50 nm particles, which show a larger yield of $[Al_2O]^+$ than $[Al]^+$. This difference likely arises from the higher percent of oxide present relative to the active Al content in the 50 nm material, the neutrals of which will deplete more of the available $[Al]^+$ in the plume, according to eq 4. The 100 nm sample has a higher active Al content relative to the amount of oxide present, which gives a higher $[Al]^+$ ion yield. Interestingly, the amount of each Al species observed for the micron-size sample is between that of

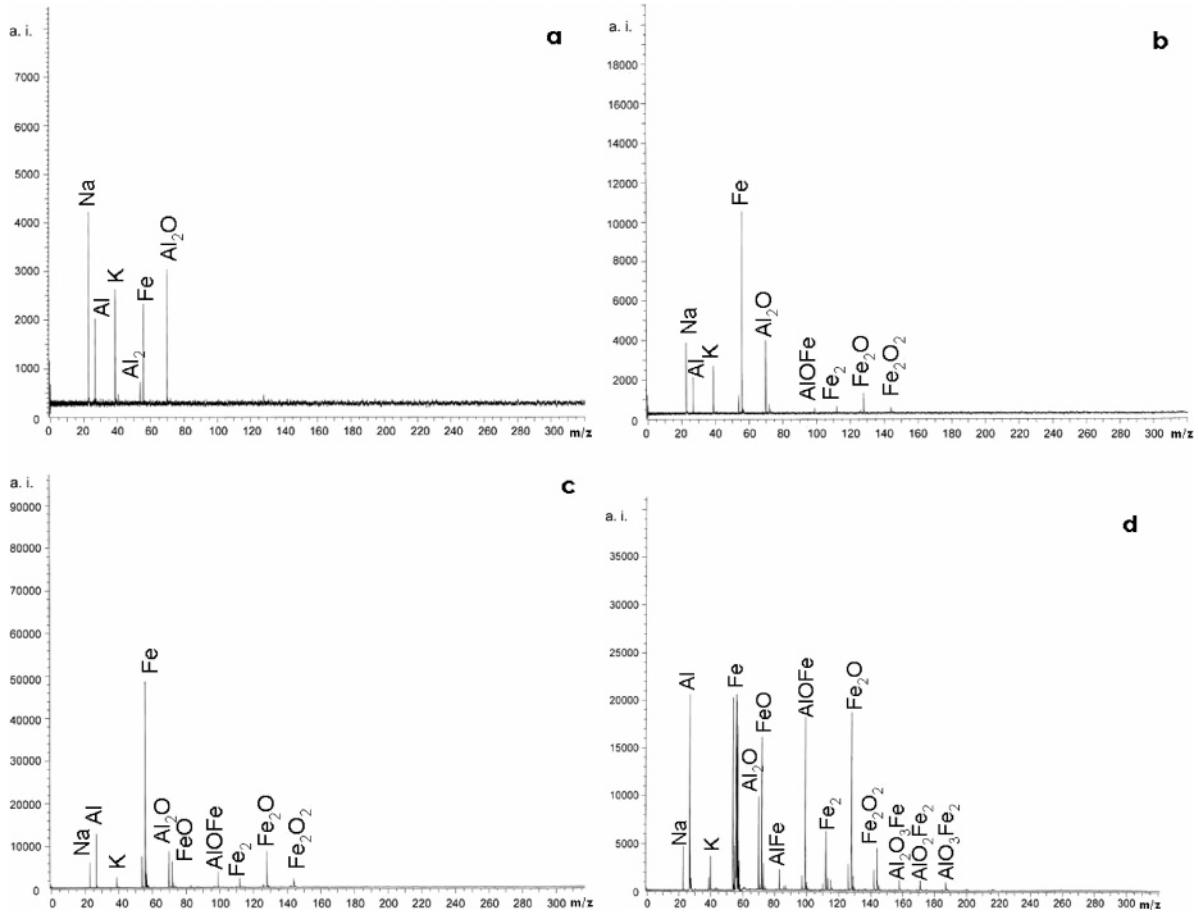

Figure 5. LDI−TOF mass spectra of thermite mixtures at a laser energy density of (a) 1.42, (b) 1.58 J/cm^2, (c) 1.74, and (d) 1.90 J/cm^2

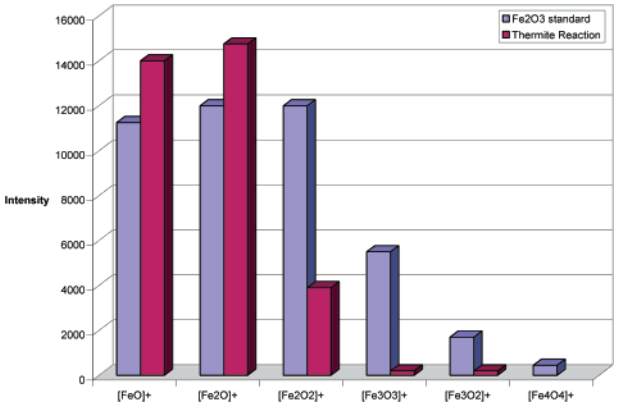

Figure 6. Relative amounts of pure iron cluster species formed during laser desorption of the Fe_2O_3 control and thermite samples at an energy density of 2.054 J/cm^2

the 50 and 100 nm samples. It yields more $[Al_2O]^+$ than the 100 nm Al, consistent with its much thicker oxide layer, but significantly less $[Al]^+$, which seems inconsistent with its high available Al content. The origin of this may lie in its higher melting point, which means that less of the heat deposited by the laser pulse is used to vaporize the sample. The power dependence of the ion yields is consistent with this suggestion. The total yield of the most prevalent ions ($[Al]^+ + [Al_2]^+ + [Al_2O]^+$) as a function of energy density (Figure 3) indicates that at the threshold, ion yields are low and relatively independent of particle size. As the power increases, the nanometer-scale particles produce the highest ion yields, which are consistent with the shorter ignition times observed in bulk materials. At the very highest energy density, however, the micron-size sample begins to exceed that of the nanoscale aluminum. The trends observed are explainable in the context of the free energy of the active Al and the oxide layer as a function of particle size. The free energy of the active aluminum in the volume becomes more positive (i.e., less stable) as the size decreases, which gives rise to the melting point depression. Conversely, the free energy of the surface oxide, which becomes the dominant contribution to the total free energy as the particles become smaller, becomes more negative, making the oxide layer more stable and, hence, less easily ablated into the plume.[17] Notably, the results are also extremely consistent with the recent melt dispersion model of Levitas et al., which suggests that the stronger oxide layer on the nanoparticles results in large pressure changes during rapid melting, causing pressure-induced spallation of the oxide layer followed by a rapid dispersion of Al clusters.[18] It is important to note that the laser-induced ignition of a thermite reaction will necessarily involve many reactions taking place in different phases of the irradiated materials. In this study, while we are observing a subset of those reactions, the species we are observing do afford support at a molecular level of the proposed advantages of nanoscale fuels on factors such as ignition time and burn rate.[8]

Irradiation of the Fe_2O_3 sample results in ionic products at a threshold power density of 1.58 J/cm^2. At the threshold, two primary species are observed, $[Fe]^+$ and $[FeO]^+$, along with K and Na impurities (Figure 4a). As the laser power is increased, more complex species are observed, in particular, $[Fe_2O]^+$ and $[Fe_2O_2]^+$, with minor products including $[Fe_2]^+$, $[Fe_3O_2]^+$, and

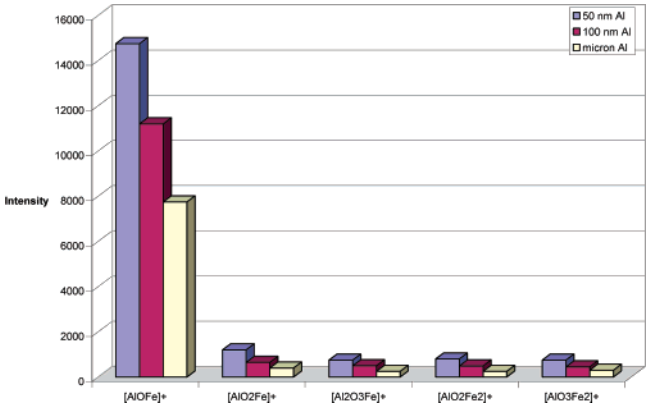

Figure 7. Mixed Al/Fe oxide species formed at an energy density of 2.054 J/cm^2 for 50 and 100 nm and micron aluminum thermite mixtures.

$[Fe_3O_3]^+$ (Figure 4b). Maunit et al. studied the laser ablation/ionization of iron oxides in considerable detail, and our spectra parallel the ones obtained by these authors under nonresonant excitation conditions and below the threshold of Fe−O bond dissociation.[19] As suggested in this previous study, neutral FeO is an important constituent of the plume and contributes to cluster formation through ion−molecule reactions. The formation of $[Fe_2]^+$ was found to be through an ion−molecule reaction between Fe^+ and neutral FeO that generates oxygen (eq 7), and FeO^+ and Fe_2O^+ are subsequently formed through an ion−molecule reaction with the generated oxygen (eqs 8 and 9)

$$Fe^+ + FeO \rightarrow Fe_2^+ + 1/2\ O_2 \quad (7)$$

$$Fe^+ + 1/2\ O_2 \rightarrow FeO^+ \quad (8)$$

$$Fe_2^+ + \frac{1}{2} O_2 \rightarrow Fe_2O^+ \quad (9)$$

The larger clusters that are formed in the plume are either oxygen deficient, $Fe(FeO)_x$, or oxygen equivalent, $(FeO)_x$, and are also formed from ion−molecule reactions between neutrals such as FeO and precursor ions.

The TOF mass spectrometry characterization of the species forming in the plumes of Al/Fe_2O_3 thermite mixtures was carried out over a range of laser powers. Of interest are species that form between the two components, which represent gas-phase reactions that are a part of the laser ignition process. No products were observed until an energy density of 1.11 J/cm^2 was reached. At this threshold, however, the only products observed were those produced from the independent components. It was not until an energy density of 1.58 J/cm^2 was reached that products consisting of Al/Fe mixed components were observed. At this threshold, small amounts of $[AlOFe]^+$ began to appear in the spectrum (Figure 5a,b). As discussed above, in the pure iron oxide, $[Fe_2O]^+$ was formed from a reaction of $[Fe_2]^+$ with O_2 (eq 9). While this reaction is possible for the formation of $[AlOFe]^+$, only trace amounts of the precursor ion, $[AlFe]^+$, were observed in the spectrum. This suggests that the $[AlOFe]^+$ likely results from an ion−molecule reaction between neutral FeO and aluminum ions (eq 10)

$$FeO + Al^+ \rightarrow FeOAl^+ \quad (10)$$

Obviously, since species such as AlO and Fe^+ are also present in the plume, their reaction may also contribute to the mixed metal product. As photothermal heating of the thermite mixture increases, more complex Al/Fe oxide species appear (Figure 5d). All of the observed clusters are aluminum-substituted analogues of the larger iron clusters; specifically, $[Al_2FeO_3]^+$ and $[AlFe_2O_3]^+$ are related to $[Fe_3O_3]^+$, while $[AlFe_2O_2]^+$ is an analogue of $[Fe_3O_2]^+$. The relative amounts of the pure iron clusters produced from the Fe_2O_3 control and from the thermite are shown in Figure 6. It can be seen that $[FeO]^+$ and $[Fe_2O]^+$ are actually produced in higher quantities in the thermite, while the larger pure iron clusters are only produced in very small amounts. This is consistent with the formation of the mixed oxide clusters at the expense of the pure iron clusters due to competition in the plume between Al^+ and Fe^+ for reaction with molecular Fe_xO_y species. The fact that $[Fe_2O]^+$ appears to be independent of the formation of $[AlOFe]^+$ is consistent with their respective formation through different mechanistic pathways.

The production of mixed metal products correlates strongly with the size of the aluminum. The energy density threshold at which mixed metal products are observed is lower for the nanoscale particles than that for the micron-scale particles (1.58 vs 1.73 J/cm^2). More significantly, the quantities of all of the mixed metal components increase with decreasing Al particle size (Figure 7). This provides direct evidence for the suggestion that the shorter ignition times that accompany smaller particle sizes are due to the lower melting point of the nanoscale materials and the active aluminum content available in the particle that, for a given laser power, produces more reactive species.

Conclusions

This study has provided insight into some of the reactions that occur between aluminum and iron oxide species in the plasma phase of the binary energetic system during laser initiation. In particular, ionic species generated directly from the laser desorption and through various ion molecules are observed for both the aluminum and iron oxide components. When the binary thermite is laser-initiated, mixed metal ionic species are produced in the plume. These species are mixed metal analogues of the iron clusters and are believed to form from competition between Al^+ and Fe^+. The amount of mixed metal clusters that form in the plasma increases as the size of the aluminum particles decreases. This provides a direct verification that the shorter ignition times observed with decreasing fuel particle size are due to a lower melting point that liberates more reactive aluminum during laser incidence.

Acknowledgment. Funding for the research was provided by AFRL/MN under Grant #FA8651-05-1-0002.

References and Notes

(1) Wang, L. L.; Munir, Z. A.; Maximov, Y. M. *J. Mater. Sci.* **1993**, *28*, 3693.
(2) Armstrong, R. W.; Baschung, B.; Booth, D. W.; Samirant, M. *Nano Lett.* **2003**, *3*, 253.
(3) Pantoya, M. L.; Granier, J. J. *Propellants, Explos., Pyrotech.* **2005**, *30*, 53.
(4) Boddington, T.; Cottrell, A.; Laye, P. G.; Singh, M. *Thermochim. Acta* **1986**, *106*, 253.
(5) Boddington, T.; Laye, P. G.; Tipping, J.; Whalley, D. *Combust. Flame* **1986**, *63*, 359.
(6) Rugunanan, R. A.; Brown, M. E. *Combust. Sci. Technol.* **1994**, *95*, 117.
(7) Bockmon, B. S.; Pantoya, M. L.; Son, S. F.; Asay, B. W.; Mang, J. T. *J. Appl. Phys.* **2005**, *98*, 064903.
(8) Granier, J. J.; Pantoya, M. L. *Combust. Flame* **2004**, *138*, 373.
(9) Ostmark, H.; Roman, N. *J. Appl. Phys.* **1993**, *73*, 1993.

(10) Wang, S. F.; Yang, Y. Q.; Sun, Z. Y.; Dlott, D. D. *Chem. Phys. Lett.* **2003**, *368*, 189.

(11) Yang, Y. Q.; Sun, Z. Y.; Wang, S. F.; Dlott, D. D. *J. Phys. Chem. B* **2003**, *107*, 4485.

(12) Moore, D. S.; Son, S. E.; Asay, B. W. *Propellants, Explos., Pyrotech.* **2004**, *29*, 106.

(13) Amoruso, S.; Bruzzese, R.; Spinelli, N.; Velotta, R. *J. Phys. B: At. Mol. Opt. Phys.* **1999**, *32*, R131.

(14) Amoruso, S.; Amodeo, A.; Berardi, V.; Bruzzese, R.; Spinelli, N.; Velotta, R. *Appl. Surf. Sci.* **1996**, *96*−*98*, 175.

(15) King, F. L.; Dunlap, B. I.; Parent, D. C. *J. Chem. Phys.* **1991**, *94*, 2578.

(16) Rosenband, V. *Combust. Flame* **2004**, *137*, 366.

(17) Kline, K. L. M. S. Thesis, University of Florida, Gainesville, FL, 2003.

(18) Levitas, V. I.; Asay, B. W.; Son, S. F.; Pantoya, M. *Appl. Phys. Lett.* **2006**, *89*, 071909.

(19) Maunit, B.; Hachimi, A.; Manuelli, P.; Calba, P. J.; Muller, J. F. *Int. J. Mass Spectrom. Ion Process.* **1996**, *156*, 173.